PHOTOINDUCTIVE IMAGING: A NEW NDE TECHNIQUE

J. C. Moulder, N. Nakagawa, K. S. No, Y. P. Lee,
and J. F. McClelland

Center for NDE and Ames Laboratory
Iowa State University
Ames, Iowa 50011

INTRODUCTION

We describe a new NDE imaging technique based on eddy current detection of thermal waves. NDE applications of thermal-wave imaging techniques using detection by photoacoustic, piezoelectric, radiometric, and optical beam deflection methods are well known [1,2]. Saniie and Luukkala [3] previously reported generating thermal waves in metals with eddy currents, but we believe this is the first instance of detecting thermal waves with an eddy current probe. Since the method depends on detecting photothermally induced changes in the inductance of an eddy current coil, we have coined the term "photoinductive imaging" to describe this new technique.

The experimental arrangement we used for carrying out photoinductive imaging is shown in Fig. 1. Thermal waves were generated in metal foils by focusing a modulated laser beam on one side of the foil, causing localized temperature-induced fluctuations in the specimen's conductivity. These were synchronously detected with an eddy current probe placed on the opposite side of the foil. Both the thermal diffusion length and the electromagnetic skin depth were large compared to foil thickness. A theory describing the interaction of thermal waves and eddy currents in thin foil specimens has been developed that shows qualitative agreement with experiment. We demonstrated the ability to form photoinductive images of thermally absorbing features on an aluminum foil by raster scanning the laser beam across black marks on the foil. We also demonstrated the capability to image a small hole in the foil. By combining two sensing modes in a single probe, photoinductive imaging offers a technique with unique advantages: eddy current signals with excellent spatial resolution, thermal wave signals using simple, noncontact detectors, and the ability to combine the two signals to improve detectability of flaws such as surface-smeared cracks.

THEORY

The photoinductive method combines two underlying physical processes, thermal diffusion and eddy current induction, each of which will be described briefly. The problem we wish to consider, shown in Fig. 1, is to calculate the change in the impedance of a single-turn coil caused by thermally induced changes in the electrical conductivity of a thin metal foil located underneath the coil. It should be noted at the outset that the present theoretical formulation is restricted to thin foils.

It is well known that the thermal diffusion process is governed by the diffusion equation. Let $T(\underline{x},t)$ be the temperature of a point $\underline{x}$ $[=(x,y)]$ on the foil at time t, relative to the environment temperature. Then, T satisfies the equation

$$\alpha \frac{\partial T}{\partial t} - \Delta^{(2)} T + \beta T = s. \tag{1}$$

Here, the first two terms constitute the usual diffusion equation except that $\Delta^{(2)}$ is the two-dimensional Laplacian. The βT term is included to account for the heat emission from the foil to the environment, and s in the RHS describes the heat source. Suppose that the source s is a chopped laser beam with the chopping frequency ω_{th}. It is practical to assume that all but the fundamental mode $e^{-i\omega_{th}t}$ are filtered out in the measurement process. If so, then it is sufficient to solve, instead of Eq. (1),

$$-\Delta^{(2)} T + k^2 T = s, \tag{2}$$

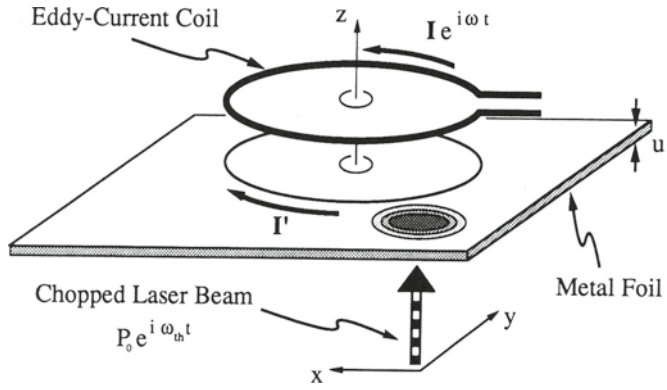

Fig. 1. Experimental arrangement for photoinductive imaging. An eddy current coil is located on one side of a metal foil. A modulated laser beam is incident on the foil from the opposite side. Scanning the laser beam over the foil produces images of flaws or any material property variations that produce thermal contrast.

where $k^2 = \beta - i\omega_{th}\alpha$. When the foil has no hole, and when s is assumed to be point-like, i.e.

$$s = s_0 \delta^2(\underline{x} - \underline{X}), \tag{3}$$

Eq. (2) can be solved immediately as

$$T(\underline{x}) = s_0 \bar{G}(\underline{x} - \underline{X}), \tag{4}$$

where $\bar{G}$ is the two-dimensional Green function written in terms of the Hankel function,

$$\bar{G}(\underline{x}) = (i/4)H_0^{(1)}(k|\underline{x}|). \tag{5}$$

Observe that $\bar{G}$ has a finite range δ_{th}, where

$$\delta_{th} = \sqrt{2}((\omega_{th}\alpha)^2+\beta^2)^{-1/4}. \tag{6}$$

We therefore see that the laser beam induces a hot spot of a finite radius δ_{th}. When δ_{th} can be regarded as small compared with other dimensions, Eq. (4) can be replaced by the simpler one,

$$T(\underline{x}) = (-s_0/k^2)\delta^2(\underline{x}-\underline{X}). \tag{7}$$

Among the parameters in (6), β is apparatus dependent. In our apparatus, it is estimated to be negligibly small. For more detailed analyses, β must be determined experimentally.

When the sample foil has a hole, a similar Green function method leads us to a boundary integral equation which must be solved somehow. When the hole is large compared with δ_{th}, one can use the local distribution (4) [or even (7)] as an approximate solution. We use Eq. (4) in our numerical analysis.

The temperature distribution T thus obtained results in a fluctuation $\Delta\sigma$ in the electrical conductivity σ via the relation

$$\Delta\sigma = (d\sigma/dT)T, \tag{8}$$

where $(d\sigma/dT)$ is the thermal gradient of σ. The fundamental observation is that this $\Delta\sigma$ can be measured by eddy-current methods.

In general, when a position dependent $\sigma(\vec{x})$ and a current distribution $\vec{j}(\vec{x})$ with a frequency ω are given, the electric fields $\vec{E}$ satisfy

$$\vec{\nabla}\times\vec{\nabla}\times\vec{E} = i\omega\mu_0[\vec{j}+(\sigma(\vec{x})-i\omega\epsilon_0)\vec{E}], \tag{9}$$

if ϵ and μ remain constant. One can always convert (9) into the integral equation

$$E_i = E_i^{(0)} + i\omega\mu_0\int d^3x' G_{ij}(\vec{x}-\vec{x}')\sigma(\vec{x}')E_j(\vec{x}'), \tag{10}$$

using the Green function

$$G_{ij} = \left(\delta_{ij}+\frac{1}{\omega^2}\partial_i\partial_j\right)\frac{e^{i\omega r/c}}{4\pi r}, \tag{11}$$

and

$$E_i^{(0)} = i\omega\mu_0\int d^3x' G_{ij}(\vec{x}-\vec{x}')j_j(\vec{x}'). \tag{12}$$

A formal solution to Eq. (11) can be given by iteration,

$$E_i = E_i^{(0)} + i\omega\mu_0\int d^3x' G_{ij}\sigma E_j^{(0)} + O((i\omega\mu_0)^2\sigma^2). \tag{13}$$

Using (13) in the impedance change ΔZ caused by σ, we find that

$$\Delta Z = \frac{(i\omega\mu_0)^2}{I^2}\int d^3x d^3x' d^3x'' j_i G_{ij}\sigma G_{jk} j_k + O((i\omega\mu_0)^3\sigma^2), \tag{14}$$

where I is the total current. Usually, formal expressions such as (13) and (14) are of little practical use. In our problem, however, (14) is useful because ΔZ can be given approximately by the first term of the expansion. Because σ exists only inside the thin foil, the shielding effect due to σ is very weak, and hence the higher order terms in the expansion are negligible. Actually, further simplification can be made because the derivative terms in (11) can be dropped when $div\vec{j} = 0$, and because $e^{i\omega r/c}$ can be set equal to one in the long-wavelength approximation. When $\vec{j}$ is a single-turn, circular coil parallel to the foil, we obtain the expression for ΔZ,

$$\Delta Z = -\left(\frac{\omega a \mu_0}{4\pi}\right)^2 \cdot \frac{d\sigma}{dT} \cdot u \cdot \int_0^{2\pi} d\theta d\theta'' \int d^2x' \frac{\cos(\theta - \theta'')}{R R''} T(\underline{x}'), \tag{15}$$

where

$$R = (a\cos 0, a\sin 0, h) - (x', y', 0), \quad R'' = (\theta \rightarrow \theta''), \tag{16}$$

and where a, h, and u are the radius of the coil, the distance between the coil and the foil, and the foil thickness, respectively. Numerical results obtained by evaluating Eq. (15) are given below.

EXPERIMENT

A schematic diagram of the apparatus is shown in Fig. 2. A commercial eddy current probe was located on one side of a metal foil. A modulated argon-ion laser, with a nominal power of 0.5 W, was focused on the opposite side of the foil. A variable-frequency mechanical chopper was used to modulate the laser, but a low-pass filter at the output of the eddyscope limited measurements to frequencies below its 100-Hz cutoff. The eddy current probe and specimen were translated relative to the laser beam with a computer-controlled x-y translator; lvdt sensors provided a position signal for the horizontal axes of a pair of x-y recorders. The analog output of a commercial eddyscope, consisting of the filtered and amplified output of the null detector of an ac bridge, was fed to a two-phase lock-in amplifier synchronized to the chopper. The magnitude and phase outputs of the lock-in were monitored with two voltmeters, whose analog output signals were summed with an lvdt signal and fed to the vertical channels of the x-y recorders to produce images. The signal represents the modulation of the impedance of the eddy current probe (on the order of 10-100 $\mu\Omega$) that is synchronous with the chopped laser. We postulate that this signal is caused by the thermally induced change in the specimen's electrical conductivity that occurs within the volume of the specimen heated by the laser beam.

Examples of the images that can be produced are shown in Fig. 3. Here we show the raster-scanned magnitude and phase images of two black stripes drawn with ink on an aluminum foil specimen 17 μm thick. A photographic image of the two stripes is shown for comparison. Notice that the streaks visible in the photographic image are reproduced in the magnitude image, giving some indication of the spatial resolution that can be obtained with this technique. Information is lacking in the phase image, only reflecting lower noise when the laser was on the black mark, which is consistent with an optically thick but thermally thin target like these ink marks. The chopper frequency was 13 Hz and the eddy current frequency was 100 kHz. At these frequencies, $\delta = 250\mu$m and $\delta_{th} = 1.8$ mm, both much greater than the foil thickness.

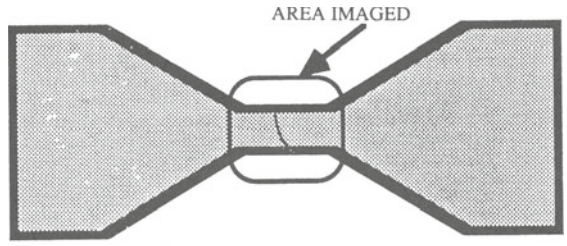

Fig. 2. Schematic diagram of the experimental apparatus.

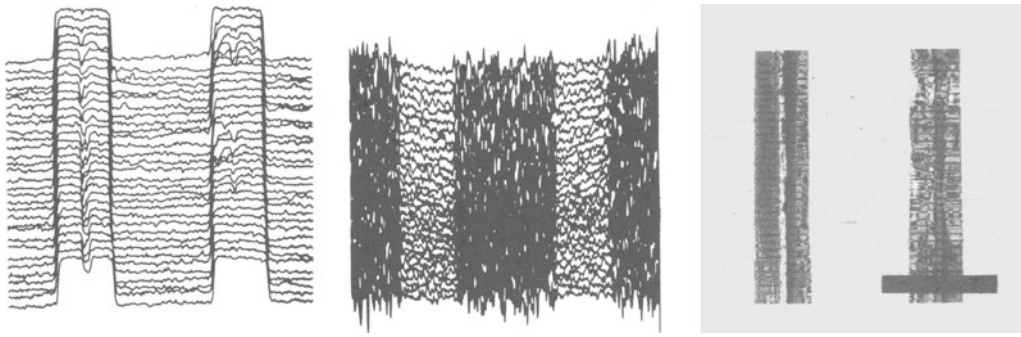

Fig. 3. Magnitude (left), phase (center), and photographic (right) images of black stripes on aluminum foil. The length of the black bar in the photograph is 1 mm. The lock-in amplifier sensitivity was 6 mV with a time constant of 125 ms.

RESULTS AND DISCUSSION

To compare experiment with predictions of the theory described above, we obtained images by scanning a blackened aluminum foil mounted on an eddy current probe relative to the fixed laser focal spot. As before, the foil was 17 μm thick; the laser chopping frequency was 13 Hz and the eddy current coil was operated at 100 kHz. The resulting magnitude image is shown in Fig. 4. The image represents the distribution of eddy currents in the foil, since the absorption of laser energy is relatively constant over the surface of the foil by virtue of the black coating of ink. Numerical results obtained by using Eq. (15) to calculate $\Delta Z(x,y)$ for a single-turn coil over a thin foil scanned by the chopped laser beam are also shown in Fig. 4. The numerical results are scaled to approximately the same size as the experimental coil. It is evident that the theoretical results are very similar to the experimental images. This qualitative agreement provides support for the postulated mechanism of thermally induced changes in conductivity.

To demonstrate the potential of the photoinductive technique for imaging flaws, numerical calculations were performed to simulate the image that would be formed by scanning the laser over a foil with a small hole. These results are shown in Fig. 5. Experimental single-line scans of the laser across a foil with and without a pinhole approximately 0.5 mm in diameter are shown in Fig. 6. In the scan over the hole, the structure in the signal at the edges of the hole is probably caused by scratches in the ink coating from the needle that was used to make the hole. A cross-section through the numerical results shows a similar shape to the experimental scan; particularly in the sharp definition of the hole's edges. This high resolution is one of the most interesting features of this technique: it provides much better resolution than could be obtained with the eddy current probe alone. In eddy current imaging, the resolution is dominated by the size of the probe (here, about 3.5 mm in diameter). In photoinductive imaging, the resolution is governed by the size of the thermal spot or, as in this case, by the diameter of the laser focal spot.

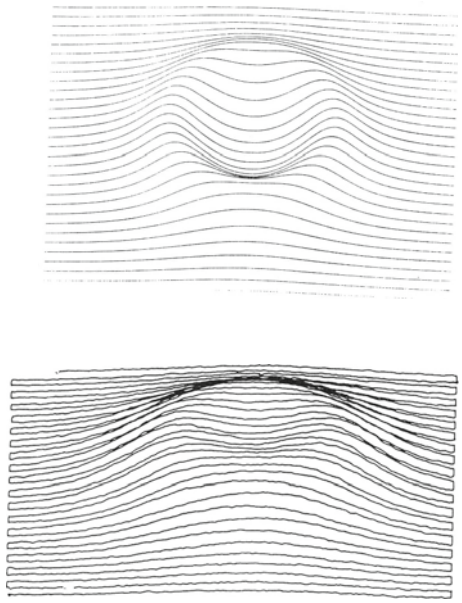

Fig. 4. (Left) Image obtained by scanning laser over stationary foil mounted on eddy current probe. The aluminum foil was painted black for uniform absorption. The image is 7.5 mm wide. (Right) Numerical calculation of photoinductive signal produced by scanning laser over a thin foil while sensing with a single-turn coil.

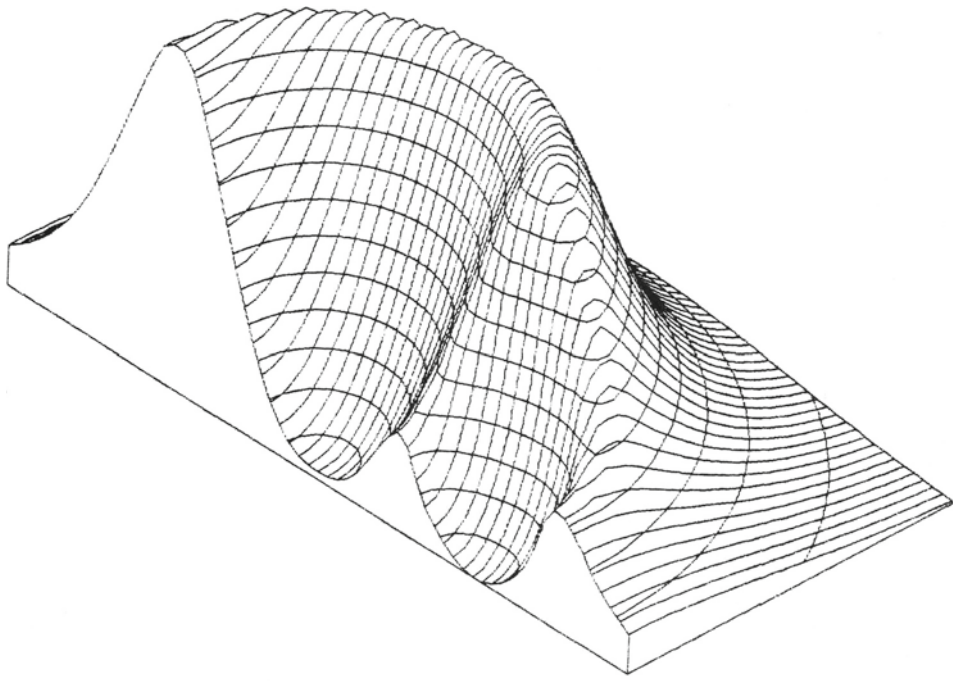

Fig. 5. Calculated photoinductive image of a foil with a hole directly under the single-turn coil.

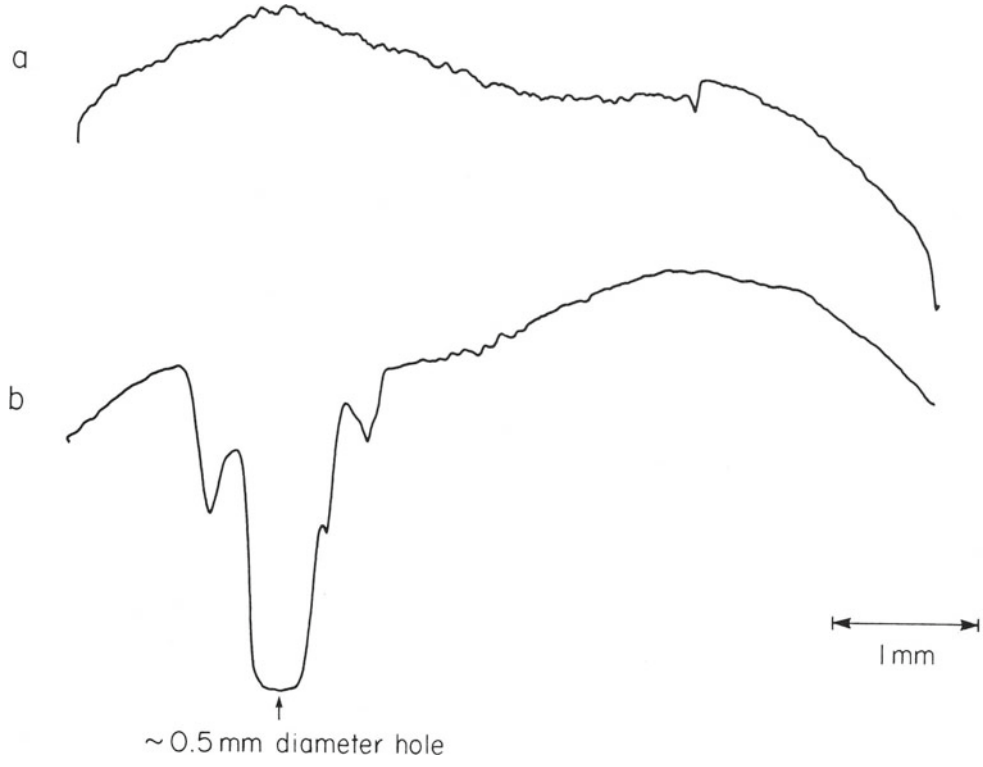

Fig. 6. Experimental line-scans of an aluminum foil specimen mounted on eddy current probe. (a) blackened foil without damage; (b) same foil with a 0.5-mm pinhole.

CONCLUSIONS

We have described a new NDE imaging technique, photoinductive imaging, based on eddy current detection of thermal waves. We have developed a theory of the effect applicable to thin foils with thickness much less than either thermal diffusion length or electromagnetic skin depth. This two-dimensional theoretical model, based on the change in specimen conductivity caused by thermal waves, agrees qualitatively with experimental measurements. Images obtained of black lines on aluminum foil suggest that resolution on the order of the laser focal spot size is attainable. Although applicable only to conductors, we feel that this method can be extended to large, thick specimens and need not be limited to foils. Signal strengths on the order of 1 to 10 mV rms referred to the input of the lock-in amplifier were obtained with a commercial eddyscope and eddy current probes. Signal-to-noise ratios were about 10 dB. Development of optimized probes and electronics is expected to yield improvements of an order of magnitude in sensitivity and signal-to-noise ratios, permitting images to be obtained in thick specimens with surface flaws.

Photoinductive imaging is a unique dual-mode NDE technique in that it combines two complementary methods: eddy currents and thermal waves. It provides two penetration depths that may be independently adjusted to infer the depth of near-surface flaws. In principle, both eddy current and photoinductive signals can be obtained from a single probe. The photoinductive method is capable of achieving resolutions comparable to the laser focal spot size, which could provide orders-of-magnitude improvement in resolution compared to typical eddy current probes. One NDE problem to which photoinductive imaging may be applicable is surface fatigue cracks that have been smeared over by mechanical surface treatments; such surface smearing can reduce the magnitude of an eddy current probe's signal, but presumably the photoinductive signal would be enhanced by the lower thermal diffusivity of the thin layer over the crack. Special eddy current probes optimized for photoinductive detection are presently being developed and exploration of the NDE applications of photoinductive imaging is underway.

ACKNOWLEDGMENT

This work was sponsored by the Center for NDE at Iowa State University and performed at the Ames Laboratory. Ames Laboratory is operated for the U. S. Dept. of Energy by Iowa State University under Contract No. W-7405-ENG-82.

REFERENCES

1. A. Rosencwaig, Photoacoustics and Photoacoustic Spectroscopy, (John Wiley, New York, 1980).

2. G. Birnbaum and G. S. White, in Research Techniques in Nondestructive Testing, edited by R. S. Sharpe (Academic Press, London, 1984), Vol. 7, pp. 259-365.

3. J. Saniie and M. Luukkala, in Review of Progress in Quantitative NDE, edited by D. O. Thompson and D. E. Chimenti, (Plenum Press, New York, 1984), Vol. 3B, pp. 769-777.